ARTICLE NO. 76-387R

J80-007

Analysis of Neutrally Stable Atmospheric Flow over a Two-Dimensional Forward-Facing Step

Walter Frost,* Juergen Bitte,† and Chih Fang Shieh‡
The University of Tennessee Space Institute, Tullahoma, Tenn.

Atmospheric flow over a two-dimensional forward-facing step is analyzed by an approach using the Navier-Stokes equations with a two-equation model of turbulence. A parametric study in the characteristic parameters of the assumed logarithmic approach velocity profile shows that an increase of the surface roughness z_0 gives rise to higher turbulence levels in the shear layer originating from the step corner. This, in turn, results in higher shear stress leading to faster reattachment of the separated flow. The typical eddy size in the shear layer increases with z_0 and causes rapid spreading of a region of high streamwise vorticity gradients.

Nomenclature

C_μ = empirical functions in expression for effective viscosity
C_D = empirical function in source term for turbulence kinetic energy equation
C_B, C_S = empirical functions in source term for ℓ equation
h = height of step
k = turbulence kinetic energy, $\frac{1}{2}(\overline{u'^2}+\overline{v'^2}+\overline{w'^2})$
ℓ = Prandtl mixing length or local turbulence length scale
n = general normal coordinate
Δn = numerical step size in n direction
Re_* = Reynolds number based on u_*, $(u_* \cdot h)/\nu$
Ro_* = Rossby number based on u_*, $u_*/(f \cdot h)$
u = velocity component in x direction
u_* = friction velocity $\sqrt{\tau_w/\rho}$
v = velocity component in y direction
w = velocity component in z direction
x = horizontal coordinate
Δx = numerical step size in x direction
x_S = horizontal extent of forward separation region defined in Fig. 5
x_R = reattachment length defined in Fig. 4
z = vertical coordinate in z plane
z_R = vertical extent of forward separation region defined in Fig. 5
Δz = numerical step size in z direction
z_0 = surface roughness
κ = von Karman constant = 0.4
μ = dynamic viscosity of the flow
ρ = density of the flow
τ = shear stress
τ_w = shear stress at surface
ψ = stream function
ω = vorticity as defined by Eq. (13)

Superscripts

$(\tilde{\ })$ = dimensionless quantity
$(\ )'$ = turbulent fluctuation about mean flow quantity

Subscripts

in = inflow condition
I,J,IN,JN = finite-difference indices as defined in Fig. 1
i,j,k = indices
out = outflow condition
P = node at which dependent variable is currently being calculated
NP = node lying adjacent to boundary mode
R = reattachment condition
S = separation condition
t = turbulent quantity

Presented as Paper 76-387 at the AIAA 9th Fluid and Plasma Dynamics Conference, San Diego, Calif., July 14-16, 1976; submitted Nov. 27, 1978; revision received April 30, 1979.

Index categories: Wind Power; Atmospheric and Space Sciences; Safety.

*Director, Atmospheric Science Division. Member AIAA.

†Assistant Professor; presently, Institute für Luft-und Raumfahrt Rheinisch-Westfälische Technische Hochschule, Aächen, West Germany.

‡Research Assistant. Member AIAA.

Introduction

WIND-INDUCED flowfields around surface obstructions, such as buildings, bridges, and other man-made structures, have long been of interest in structural design. Operating low-speed aircraft between buildings in regions of steep velocity gradients, large fluctuations through vortex fields, or recirculation zones is very hazardous. In order to take precautions against these hazards, a clear understanding of the flowfield around the geometries of typical buildings is required for the design of airports for V/STOL aircraft or helicopter ports in large metropolitan areas.

Predicting the gross flow features and time mean values in turbulent flows requires the solution of the governing Reynolds equation subject to known boundary conditions. Due to the considerable progress in numerical techniques in recent years,[1-3] the governing system of equations can be solved fairly readily. The major remaining problem is that of finding a model for the Reynolds stress to close the system of conservation equations. This is done traditionally by assuming a linear relationship between the Reynolds stress and the local mean rate of strain, with the coefficient of proportionality given by the turbulent viscosity. The latter can then be determined either by empirical algebraic relations, such as the Prandtl mixing length, or from the solution of additional differential equations for one or more properties of the turbulent motion. Mixing length models have been widely used and have provided useful results for simple boundary-layer-type turbulent flows. For more complex flows which include separation and recirculation, however, such models cannot accurately predict the flowfield. Since they are based

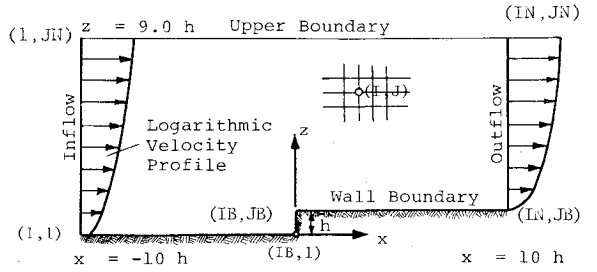

Fig. 1a Description of flow region considered and of numerical coordinate system used.

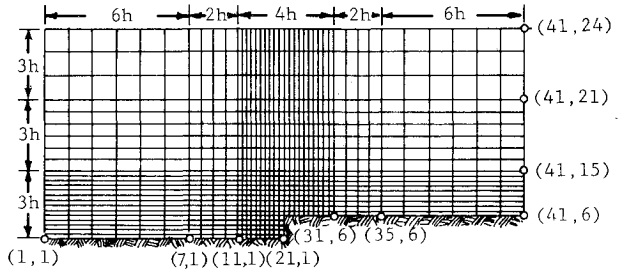

Fig. 1b Actual grid distribution.

on local flow properties, they cannot adequately account for the convective character of turbulence. Therefore, the closure model employed in this investigation uses two differential equations for the determination of the turbulence properties. The model was developed by Gosman et al.[1] and is based on the turbulence kinetic energy k concept proposed by Prandtl[4] and Kolmogorov[5] with a transport equation for the turbulence length scale ℓ derived by Rotta.[6] The model is generally referred to as a two-equation model of turbulence, since two differential equations for k and ℓ are solved along with the other governing equations.

In the present paper, the turbulence flow model is utilized in the analysis of neutrally stable atmospheric flow over a two-dimensional forward-facing step, as shown in Fig. 1. The atmospheric motion far upstream of the step is described by a logarithmic velocity profile

$$\frac{u}{u_*} = \frac{1}{\kappa} \cdot \ell n \left(1 + \frac{z}{z_0}\right) \tag{1}$$

where u_* is the friction velocity defined in terms of the surface shear stress τ_w

$$u_*^2 = \tau_w / \rho$$

κ is the von Karman constant of value 0.4, and z_0 is the surface roughness parameter.

The effect of this flowfield around the forward-facing step of variations in the parameters u_* and z_0 which characterize the approach velocity profile in the atmospheric boundary layer is investigated and discussed.

Governing Equations

The turbulent mean flow equations for the two-dimensional atmospheric surface layer utilized in this study are described in detail in Ref. 2. The turbulence model employed requires the determination of asymptotic constants C_μ, C_D, C_B, and C_S contained in the transport equations which appear in the source terms for turbulence kinetic energy k and for turbulence length scale ℓ. The transport equations for k and ℓ can be written as[1,2]:

$$u_j \frac{\partial k}{\partial x_j} = \frac{1}{\rho} \frac{\partial}{\partial x_j} \left((\mu + \mu_t) \frac{\partial k}{\partial x_j} \right) + \mu_t \frac{\partial u_i}{\partial x_j} D_{ji} - C_D \frac{k^{3/2}}{\ell} \tag{2}$$

$$u_j \frac{\ell}{\partial x_j} = \frac{1}{\rho} \frac{\partial}{\partial x_j} \left((\mu + \mu_t) \frac{\partial \ell}{\partial x_j} \right) - C_B \mu_t \frac{\partial u_i}{\partial x_j} D_{ji} + C_s k^{1/2} \tag{3}$$

where the eddy viscosity μ_t is modeled by $C_\mu k^{1/2} \ell$ and D_{ji} equals $(\partial u_i/\partial x_j) + (\partial u_j/\partial x_i)$. Since the governing equations should hold for the entire flowfield, the preliminary estimation of these constants is conventionally carried out by a wall region approximation. Considering a constant shear layer in which the mixing length hypothesis is applicable,

$$\ell = \kappa (z + z_0) \tag{4}$$

and assuming that the production and dissipation of turbulence kinetic energy is locally in equilibrium, which holds at least in the wall regions,[7] we obtained

$$C_\mu = u_* / k^{1/2} \tag{5}$$

and

$$C_D = C_\mu^3 \tag{6}$$

For a neutral atmosphere, it has been determined experimentally and reported by Fichtl[8] that

$$k = 5.78\, u_*^2 \tag{7}$$

Assuming that this is true for the surface layer where τ is constant, we obtain from Eqs. (5-7)

$$C_\mu = 0.416 \qquad C_D = 0.072 \tag{8}$$

In the vicinity of the wall, one may expect the convection of turbulence length scale to be negligible. In two-dimensional wall regions, Eq. (3) is thus reduced to

$$\frac{\partial}{\partial z} \left[C_\mu \rho k^{1/2} \ell \frac{\partial \ell}{\partial z} \right] + C_S \rho k^{1/2} - C_\mu C_B \rho \ell^2 \left(\frac{\partial u}{\partial z} \right)^2 k^{-1/2} = 0 \tag{9}$$

Introducing Eqs. (1), (4), and (5) into Eq. (9) gives

$$C_B = \frac{\kappa^2 \cdot C_\mu}{C_D} + \frac{C_S}{C_D}$$

An expression for C_S has been developed previously for the case of homogeneous turbulence behind a grid.[7] Since the governing equations must reduce to all possible flow conditions, it is expected that this relationship will also hold for the atmospheric boundary layer

$$C_S = 0.5 (C_D / C_{\mu 0}) \tag{10}$$

such that

$$C_S = 0.087 \qquad C_B = 2.133 \tag{11}$$

Together with Eq. (8), this yields a set of preliminarily estimated constants to be confirmed and possibly adjusted as experimental data become available.

Numerical Solution

Numerical Procedure

The mathematical problem posed in this paper has been solved by utilizing the numerical procedure of Gosman et al.[1] This solution algorithm utilizes the stream function ψ and the vorticity ω variables; therefore solutions are obtained without requiring information about the pressure gradients. The governing equations can be expressed in the common form of an elliptical partial-differential equation suitable for simultaneous numerical integration.[1,2] This differential equation is then replaced by an algebraic finite-difference equation, which is obtained by integration over finite areas rather than Taylor series expansion, assuring a broader range

of applicability especially in nonrectangular coordinate systems.[1] The diffusion and source terms are expressed in a weighted central-difference form.

The integration of the convection terms employs "upwind differencing," a one-sided rather than centered space differencing, where the scheme is backward when the velocity is positive and forward when it is negative. This formulation of the first-order terms gives greater numerical stability than can be obtained with central differences.[9] Roache[10] indicates that the application of the "upwind differencing" technique may introduce an artificial viscosity. This pseudo-viscosity, however, can be reduced by decreasing the grid size used in the numerical programming.

No computer runs were made specifically to estimate the effects of artificial viscosity. The following subjective arguments, however, suggest these effects are not excessive. The no-slip condition employed at the wall insures that no pseudo-viscosity is created there. In the flowfield far from the wall, the artificial viscosity estimated from the undisturbed upstream conditions is about the same as the eddy viscosity. Since the effect of pseudo-viscosity can be thought of as reducing the effective velocity appearing in the advective terms of the transport equations,[10] the same magnitude of eddy viscosity and pseudo-viscosity simply cancels the advection terms from the transport equations of the vorticity, the turbulence kinetic energy, and its length scale. This, of course, corresponds to the case of uniform flow properties and conditions near upper boundary where perturbation from the surface irregularity is negligible. In the intermediate regions of the flowfield, the pseudo-viscosity is estimated to be about 20% of the eddy viscosity. The effect of this pseudo-viscosity, however, on the numerical solution is often small.[10] The grid spacing distribution is shown in Fig. 1b for the convenience of the reader in estimating the magnitude of the pseudo-viscosity in the flowfield computed. The flowfield is separated into regions, Fig. 1b, and nodes are equally spaced throughout the regions.

Because of the nonlinear character of the resulting finite-difference equations, they are solved by an iterative, successive substitution technique.[1]

The physical coordinate system was chosen such that the origin was located at the lower step corner, with the positive x axis pointing in the downstream direction parallel to the wall. The z axis is normal to the x axis and is aligned with the front face of the step (see Fig. 1). In this coordinate system the flow regime considered extends ten step heights in the upstream and downstream directions and nine step heights in the vertical direction. The origin of the numerical coordinates was situated at the lower left corner of the flowfield with I indexing in the x direction and J indexing in the z direction. A variable mesh was used which gradually decreased in size near the wall and in the vicinity of the step. In the iteration process, the field was swept from left to right beginning at the wall and proceeding in the increasing J direction.

Boundary Conditions

Due to the elliptical nature of the flow problem, boundary conditions are prescribed along the entire boundary of the flow regime, i.e., following Fig. 1 along the inlet, the outlet, and the upper and lower boundaries (walls). All conditions are either of Dirichlet or Neumann type.

Inflow

At the inflow, a logarithmic velocity profile, [Eq. (1)] is assumed. The ψ boundary condition can then be determined by integrating the velocity profile (1) over the inlet height

$$\psi(z) = \rho \frac{u_*}{k}\left[(z+z_0)\ln\left(1+\frac{z}{z_0}\right)+z\right] \tag{12}$$

The condition for the vorticity ω is

$$\omega(z) = \frac{\partial w}{\partial x} - \frac{\partial u}{\partial z} \tag{13}$$

where the last term can be calculated from the specified logarithmic velocity profile as

$$\frac{\partial u}{\partial z} = \frac{1}{\rho}\frac{\partial^2 \psi}{\partial z^2} = \frac{u_*}{\kappa}\frac{1}{z+z_0}$$

The remaining term of the inflow vorticity was allowed to develop as part of the solution by approximating[10]

$$\frac{\partial^2 w}{\partial x^2} = 0 \tag{14}$$

and setting

$$\left.\frac{\partial w}{\partial x}\right|_{1,J} = \left.\frac{\partial w}{\partial x}\right|_{2,J} = -\left.\frac{1}{\rho}\frac{\partial^2 \psi}{\partial x^2}\right|_{2,J} \tag{15}$$

The boundary condition employed for the turbulence kinetic energy k was derived from the shear distribution[11]

$$\tau_t(z) = -\rho\overline{u'w'} = \rho u_*^2\left[1-\frac{A}{\kappa}\cdot\frac{f(z+z_0)}{u_*}\right]$$

where f is Coriolis force and A is assigned a value 5.0. In terms of the Prandtl-Kolmogorov formulation, one can write

$$\tau_t(z) = \rho k^{1/2}\ell C_\mu \frac{\partial u}{\partial z}$$

Equating the two and substituting the velocity gradient from Eq. (1), one obtains the boundary conditions for k at the inlet as

$$k = \left[\frac{u_*}{C_\mu}\right]^2\cdot\left[1-\frac{A}{\kappa}\frac{f(z+z_0)}{u_*}\right]^2 \tag{16}$$

The corresponding condition on the turbulence length scale is then

$$\ell = \kappa(z+z_0) \tag{17}$$

Outflow

The assumption for ψ was that $\partial w/\partial x = 0$, or

$$\left.\frac{\partial^2 \psi}{\partial x^2}\right|_{IN,J} = \left.\frac{\partial^2 \psi}{\partial x^2}\right|_{IN-1,J} = \left.\frac{\psi_{IN}-2\psi_{IN-1}+\psi_{IN-2}}{(\Delta x)^2}\right|_J$$

which yields

$$\psi_{IN,J} = 2\psi_{IN-1} - \psi_{IN-2} \tag{18}$$

For the vorticity, it is assumed that the gradient in the flow direction vanishes, i.e.,

$$\partial\omega/\partial x = 0 \tag{19}$$

Similar conditions were imposed for the kinetic energy and length scale

$$\partial k/\partial x = 0 \tag{20}$$

$$\partial \ell/\partial x = 0 \tag{21}$$

Upper Boundary

The location of the upper boundary was assumed far enough out that velocity deflections caused by the step were negligibly small. Consequently, the streamline condition is

$$\partial\psi/\partial x=0 \tag{22}$$

i.e., w is zero crossing the upper boundary.

The vorticity condition imposed was that of a vanishing gradient

$$\partial\omega/\partial z=0 \tag{23}$$

which was also required for the turbulence kinetic energy. However, in the horizontal or x direction

$$\partial k/\partial x=0 \tag{24}$$

The length scale was prescribed as

$$\partial\ell/\partial x=0 \tag{25}$$

Wall Boundary

As the flow is parallel to the wall, the boundary condition for the stream function is:

$$\psi=0 \tag{26}$$

The vorticity boundary condition is more problematic as it essentially drives the flow. It can be derived from a Taylor-series expansion of the stream function around a near wall point (NP), Δn away from the wall, in terms of the wall point (P) conditions. Details are given in Refs. 1, 2, and 10. The final form is:

$$\omega_P=-\frac{3(\psi_{NP}-\psi_P)}{(\Delta n)^2\cdot\rho}-\frac{1}{2}\omega_{NP} \tag{27}$$

The turbulence kinetic energy specification along the wall was derived from the wall inlet condition of

$$k_{\text{in}}=(u_*/C_{\mu 0})^2 \tag{28}$$

It was assumed that k obeyed Eq. (30) along the entire wall; however, with u_* varying as

$$u_*|_{\text{wall}}=\ell\left.\frac{\partial u}{\partial z}\right|_{\text{wall}} \tag{29}$$

implying a logarithmic velocity profile from the wall to the first interior node. Furthermore, at the wall,

$$u_*|_{\text{wall}}=\kappa\cdot z_0\cdot(-\omega) \tag{30}$$

or

$$k^*_{\text{wall}}=(\kappa\cdot z_0\cdot\omega/C_\mu)^2 \tag{31}$$

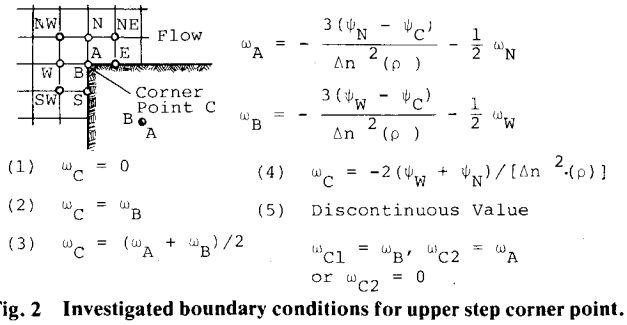

Fig. 2 Investigated boundary conditions for upper step corner point.

The length scale at the wall was prescribed by

$$\ell=\kappa\cdot z_0 \tag{32}$$

Special Treatment at Step Corner

The stream function at the upper corner like the rest of the wall is $\psi_C=0$. Similarly, k_C and ℓ_C are uniquely prescribed by the lower boundary condition. However, there are several alternatives for the evaluation of ω_C. Referring to Fig. 2, one can apply Eq. (27) either to the upstream side (face) of the step

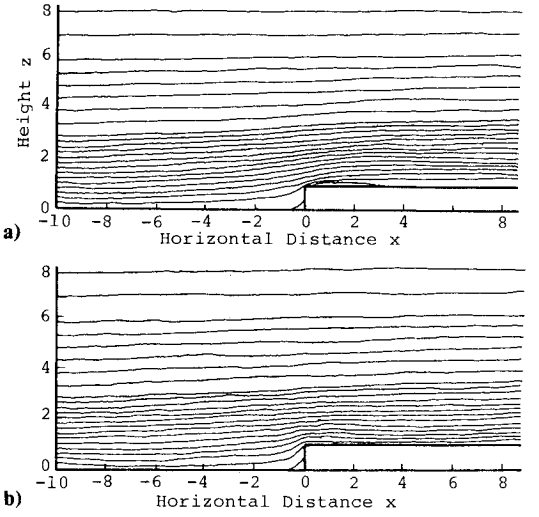

Fig. 3 Stream function pattern for a) $\tilde{z}_0=0.005$ and b) $\tilde{z}_0=0.1$.

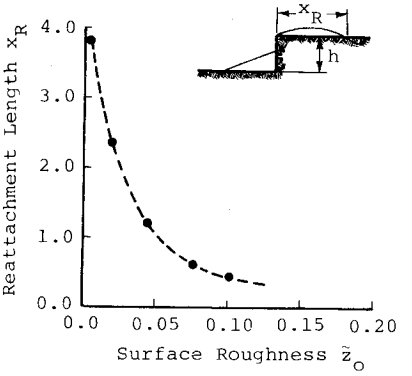

Fig. 4 Reattachment length of top separation region in dependence of $\tilde{z}_0$.

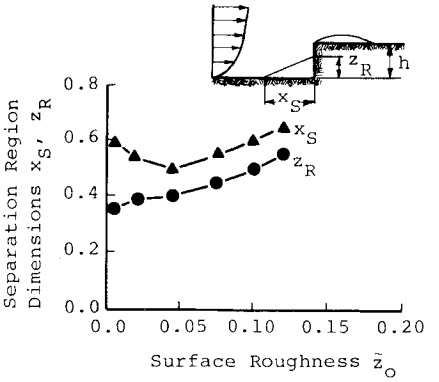

Fig. 5 Forward separation region geometry in dependence of $\tilde{z}_0$.

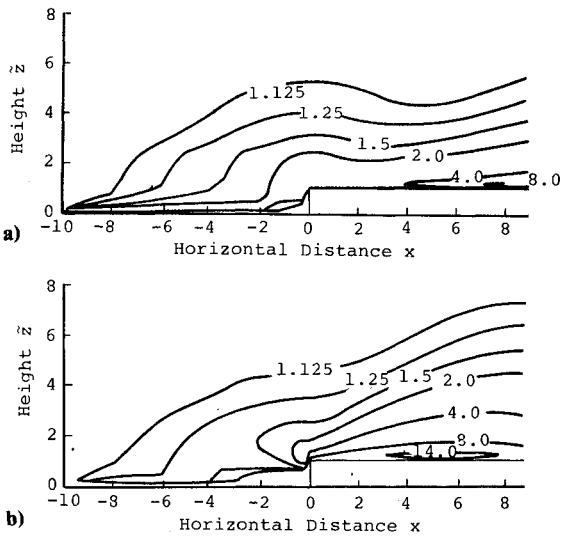

Fig. 6 Turbulence kinetic energy contours for a) $\tilde{z}_0 = 0.005$ and b) $\tilde{z}_0 = 0.1$.

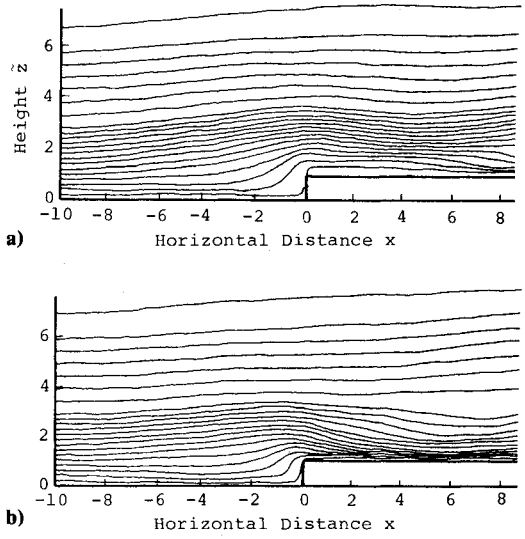

Fig. 7 Lines of constant turbulence length scale for a) $\tilde{z}_0 = 0.005$ and b) $\tilde{z}_0 = 0.1$.

or to the downstream wall obtaining, respectively:

$$\omega_C = \omega_A = -\frac{3\psi_N}{\rho(\Delta z)^2} - \frac{1}{2}\omega_N \tag{33}$$

and

$$\omega_C = \omega_B = -\frac{3\psi_W}{\rho(\Delta x)^2} - \frac{1}{2}\omega_W \tag{34}$$

There are also other possibilities. Seven different methods are given in Ref. 10, and most of these (listed in Fig. 2) were investigated in the present study. Method 1 represents an attempt to force separation at the corner, assuming that the vorticity vanishes at a separation point. Method 2 is based on the idea that, since separation occurs tangentially to the upstream wall, upstream wall evaluation should be used. Method 3 is an attempt to average out both values, while method 4 is derived from adding both values in a first-order formulation. Method 5 arises from the argument that no continuity of ω can be expected for the geometric singularity of the corner.

When applied to a laminar flow case, obtained by setting the turbulent viscosity equal to zero, all methods functioned well and enforced separation from the corner. The second formulation, however, was the most effective in producing a well-developed realistic separation region. For this reason, it was used in all subsequent calculations.

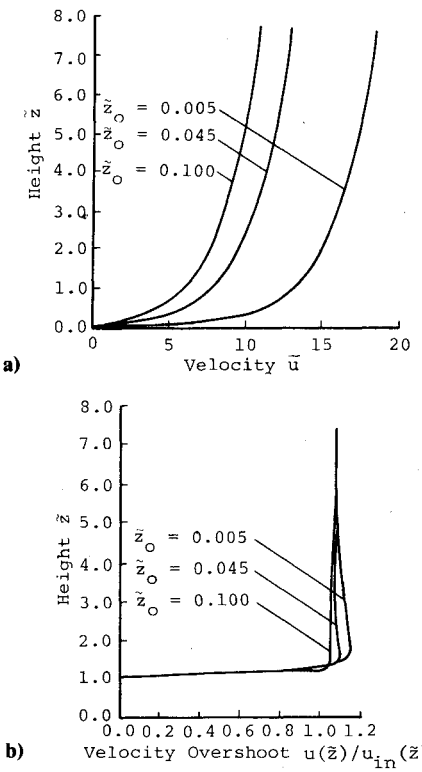

Fig. 8 Velocity profiles for various $\tilde{z}_0$: a) approach velocities; b) velocity overshoot at $x = 0$; $\tilde{z}$ is the dimensionless height above natural terrain upstream.

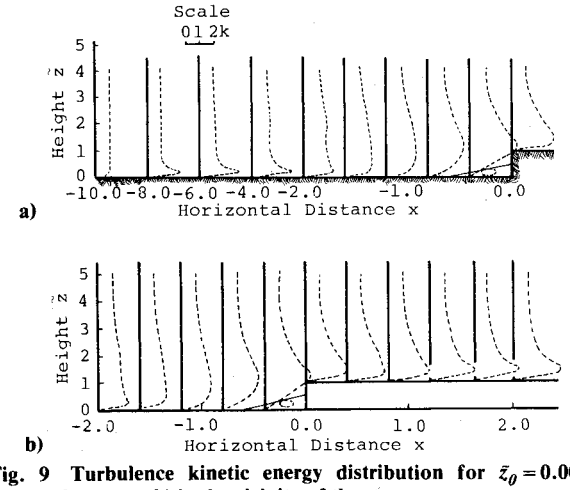

Fig. 9 Turbulence kinetic energy distribution for $\tilde{z}_0 = 0.005$: a) ahead of the step; b) in the vicinity of the step.

Flow Parameters

A nondimensional form of the governing equations was obtained by adopting the step height h as the characteristic length and the friction velocity u_* as the characteristic velocity. These were introduced into the governing equation described in detail in Refs. 1 and 2. The problem thus reduces from one of four dimensional parameters, u_*, f, z_0, and h, to three dimensionless groups, $\tilde{z}_0$, Ro_*, and $1/Re_*$.

$$\tilde{z}_0 = \frac{z_0}{h}; \quad Ro_* = \frac{u_*}{f \cdot h}; \quad Re_* = \frac{\rho u_* h}{\mu}$$

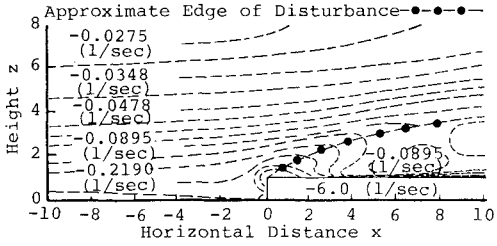

Fig. 10 Vorticity distribution for $\tilde{z}_0 = 0.045$.

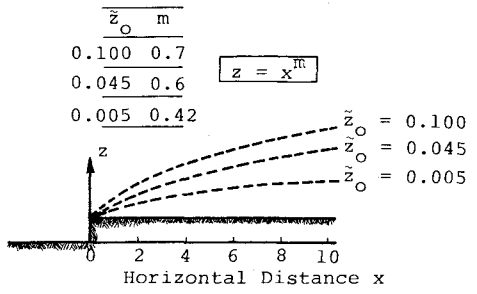

Fig. 11 Variation of outer edge of vorticity wake region for different $\tilde{z}_0$.

However, for atmospheric flow, the value of the molecular viscosity is much smaller than the eddy viscosity, $\mu \ll \mu_t$, thus the flow problem becomes essentially independent of Re_* in the atmospheric surface layer where the Coriolis force is negligible. Therefore, the only remaining significant parameter is $\tilde{z}_0$.

Results and Discussion

In the subsequent study, calculations were carried out for the following five values of $\tilde{z}_0$ with the Rossby number kept constant at $Ro_* = 750$: 1) $\tilde{z}_0 = 0.005$, 2) $\tilde{z}_0 = 0.020$, 3) $\tilde{z}_0 = 0.045$, 4) $\tilde{z}_0 = 0.075$, and 5) $\tilde{z}_0 = 0.100$. The resulting ψ, k and ℓ distributions for the two extreme cases 1 and 5 are shown in Figs. 3-11. It is emphasized here that variation in $\tilde{z}_0$ gives corresponding variations in the wind velocity profiles of the approaching flow. The smaller the $\tilde{z}_0$, the greater the wind shear near the wall (Fig. 8a).

Comparing the various streamline patterns, one notices that the shapes of the upstream and downstream separation regions vary with $\tilde{z}_0$. While the top reattachment length x_R changes substantially, the front separation distance x_S varies only slightly. Figures 4 and 5 show the geometry of the separation and reattachment regions as characterized by the distances x_S, z_R, and x_R.

The reattachment length x_R was found to increase with decreasing $\tilde{z}_0$, indicating that a smoother surface or larger step height would delay reattachment of the flow on top of the step. The reason for this is readily understood by looking at the respective TKE and ℓ contour plots in Figs. 6 and 7. For smaller $\tilde{z}_0$, the turbulence intensities and length scale are seen to decrease in the upstream and downstream vicinity of the upper step corner. This is a result of the higher flow acceleration created by the displacement of a fuller approach velocity profile containing higher momentum near the wall (see also Fig. 8b). Acceleration in the flow is generally known to diminish turbulence production and to reduce the turbulence length scale or typical eddy size by means of vortex stretching. These lower turbulence intensities, together with the reduced length scale, lead to a lower effective viscosity or shear on top of the step, delaying reattachment and causing x_R to increase. This result suggests that wind approaching over water or smooth asphalt prior to impinging on a long, low building would produce longer separation regions on the roof. These separation regions, which are hazardous to a VTOL aircraft landing on the roof, can conceivably be broken up by roughing the surface around the landing pad (for example, plant numerous trees about the building).

For the forward separation region, the situation is somewhat different. Except for a small region in the lower $\tilde{z}_0$ range, the bubble is found to grow in size with increasing surface roughness, even though the maximum vorticity occurring inside the bubble decreases. In the $\tilde{z}_0$ range under consideration, where the vorticity decreases only slightly, the growth of the bubble seems to be influenced largely by the growth of the turbulence length scale. However, in the lower $\tilde{z}_0$ range mentioned previously, the steep decline of vorticity seems to be more influential than the growth of the length scale, resulting in a partial reduction of bubble size.

More information is contained in the gradients of the stream function, i.e., the velocity distributions. Figure 8 indicates how the presence of the step affects the horizontal velocity profile at $x = 0.0$ for the different roughness parameters. The profile with the strongest velocity gradient at the wall and the highest momentum near the surface produces the largest velocity overshoot. This is easily perceived because for the smaller $\tilde{z}_0$, the flow carries more mass near the wall, which is suddenly displaced by the step, creating a locally accelerated flow region. The overshoot is in accordance with the lower shear predictions and longer reattachment lengths for the smaller $\tilde{z}_0$. It is reported that the velocity speed-up ratio, defined as the local speed at a height above the elevated step height downstream, divided by the undisturbed speed at the same height above the natural terrain upstream is increased with increasing $\tilde{z}_0$.[13-15] Calculating the speed-up ratio, as defined earlier from Fig. 8, we obtained 1.45 for $\tilde{z}_0 = 0.005$ and 1.65 for $\tilde{z}_0 = 0.10$ near the step surface. These are comparable with the empirical results; 1.7-1.8 for rough surface and 1.4-1.5 for smooth surface reported in Ref. 15.

The turbulence kinetic energy contours in Fig. 6 reveal that for increasing $\tilde{z}_0$, the turbulence energy levels in the shear layer growing from the step corner rise accordingly. Likewise, the turbulent viscosity and with it the turbulent shear stress increase in unison. This further verifies once more why smaller surface roughness produces bigger overshoot and larger downstream separation regions.

Figure 9 gives a set of turbulence intensity profiles over the whole flowfield for $\tilde{z}_0 = 0.005$. These profiles essentially agree with the findings of Taulbee and Robertson.[12] One observes that high-turbulence intensity extends throughout a region about ½-⅝ h above the top surface of the step. If the forward-facing step were a landing pad, the sharp leading edge would create high turbulence directly in the touchdown zones. Further study on the effects of rounding the leading edge or installing parapets would be useful to heliport design.

The turbulence length scale plots (Fig. 7) expose how different the distributions actually can become from the linear variation often assumed. The downstream influence of the step on the turbulence structure is recognized by the growth in ℓ, indicating an increase of typical eddy size in the spreading shear layer.

From the four variables, ω, ψ, κ, and ℓ, the vorticity and the $\tilde{z}_0$ influence on it has not yet been discussed. Figure 10 shows the vorticity contours for $\tilde{z}_0 = 0.045$. It is pointed out thata disturbance region with locally high-streamwise vorticity gradients is formed and spreads downstream parabolically. Figure 11 shows how a surface roughness change affects the extent of this region of high vorticity. It is seen that a $\tilde{z}_0$ increase generates a wider spread, possibly as a consequence of the changes in the turbulence structure (larger eddies) of the shear layer discussed in the previous paragraph. The influence of vorticity in the atmosphere on aircraft flight has not been analyzed to any great extent. One observes, however, that strong vorticity effects extend farther above the building than either the velocity or turbulence disturbances. This may prove to be a significant factor in VTOL operations in urban areas.

Conclusion

The results of this study indicate that the two-equation turbulence model described herein provides prediction of the wind field over a bluff geometry surface that shows agreement with physical intuition and the limited experimental data available (primarily wind tunnel data).

The value of the empirical coefficients used in the turbulence transport equations are $C_\mu = 0.416$, $C_D = 0.072$, $C_S = 0.087$, and $C_B = 2.133$. These values satisfy the upstream, undisturbed, logarithmic wind profiles and give meaningful results in the disturbed flow about the building.

The dimensionless wind field depends on the Rossby number Ro_*, which was fixed in the present study, and the surface roughness $\bar{z}_0$. One may summarize the effects of $\bar{z}_0$ by stating that in the downstream flow region an increase in $\bar{z}_0$ gives rise to higher turbulence levels in the shear layer originating from the step corner. This, in turn, results in higher shear stress leading to fast reattachment. The typical eddy size in the shear layer increases with $\bar{z}_0$ and causes rapid spreading of a region of high-streamwise vorticity gradients. In the upstream flow region, changes in $\bar{z}_0$ have only moderate influence on the flow parameters. Except for very small surface roughness, the front separation bubble grows in size for increasing $\bar{z}_0$.

Acknowledgments

The research reported herein was supported by NASA Contract NAS8-29584. G. H. Fichtl and D. W. Camp of the Aerospace Environment Division, Space Sciences Laboratory, Marshall Space Flight Center, were the scientific monitors, and support was provided by J. Enders of the Aeronautical Systems Division, Transport Aircraft Programs Office, NASA Headquarters.

References

[1] Gosman, A. D., Pun, W. M., Runchal, A. K., Spalding, D. B., and Wolfshtein, M., *Heat and Mass Transfer in Recirculating Flows*, Academic Press, New York, 1973.

[2] Bitte, J. and Frost, W., "Atmospheric Flow over Two-Dimensional Bluff Surface Obstructions," NASA CR-2750, Oct. 1976.

[3] *Symposium on Turbulent Shear Flow*, Vol. 1, University Park, Pa., April 18-20, 1977.

[4] Prandtl, L., "Ueber ein neues Formelsystem fuer die Ausgebildete Turbulenz," Nachrichten von der Akademie der Wissenschaften in Göttingen, *Math. Physis. Kl.*, Van den Loeck und Ruprecht, Göttingen, 1945, pp. 6-19.

[5] Kolmogorov, A. M., "Equations of Turbulent Motion of an Incompressible Turbulent Fluid," *Izvestiya Akademii Nauk Uzbekskoi SSR Series Phys. VI*, No. 1-2, 1942, pp. 56-58; translated into English at Imperial College, Mechanical Engineering Dept. Rept. ON/6, 1968.

[6] Rotta, J. C., "Statistische Theorie Nichthomogener Turbulenz," *Zeitschrift für Physik*, Vol. 129, pp. 547-572, and Vol. 131, pp. 51-77, 1951; also, English translation at Imperial College Mechanical Engineering Department Repts. TWF/TN/38 and TWF/TN/39, London, 1951.

[7] Launder, B. E. and Spalding, D. B., *Mathematical Models of Turbulence*, Academic Press, New York, 1972.

[8] Fichtl, G. H., "Problems in the Simulation of Atmospheric Boundary Layer Flows," AGARD CP-140, 1973.

[9] Courant, R., Isaacson, E., and Rees, M., "On the Solution of Non-Linear Hyperbolic Differential Equations by Finite Differences," *Communications on Pure and Applied Mathematics*, Vol. 5, p. 243.

[10] Roache, P. J., *Computational Fluid Dynamics*, Hermosa Publishers, Albuquerque, N. Mex., 1972.

[11] Tennekes, H., "The Logarithmic Wind Profile," *Journal of Atmospheric Sciences*, Vol. 30, 1973, pp. 234-238.

[12] Taulbee, D. B. and Robertson, J. M., "Turbulent Separation Analysis Ahead of a Step," ASME Paper 71-WA/FE-32, Washington, D.C., Nov. 1971.

[13] Gorlin, S. M., Ziborova, S. P., and Timoshuk, L. T., "Studies of Flow Past a Protrusion with Varying Underlying Surface Roughness," *Certain Problems of Experimental Aerodynamics*, edited by S. M. Gorlin, NASA TT F-16565, Nov. 1975, pp. 1-23.

[14] Meroney, R. N., Sandborn, V. A., Bouwmeester, R.J.B., Chien, H. C., and Rider, M., "Sites for Wind Power Installations: Physical Modeling of the Influence of Hills, Ridges and Complex Terrain on Wind Speed and Turbulence," Draft Final Rept.: Pt. III, Fluid Mechanics and Wind Engineering Program, Colorado State University, Fort Collins, Colo., June 1978, pp. 70-71.

[15] Bowen, A. J. and Lindley, D., "A Wind Tunnel Investigation of the Wind Speed and Turbulence Characteristics Close to the Ground over Various Escarpment Shapes," *Boundary-Layer Meteorology*, Vol. 12, Issue 3, 1977, pp. 259-271.